RESEARCH PAPER

Hydrogels for dental pulp repair: enhancing physicochemical and regenerative potential with CaP-loaded alginate-gelatin hydrogel scaffolds: a FEM and ANN modeling

Abbasali Khademi[1]*, Amirsalar Khandan[1], Pedram Iranmanesh[1]

[1]Department of Endodontics, Dental Research Center, Dental Research Institute, School of Dentistry, Isfahan University of Medical Sciences, Isfahan, Iran

ABSTRACT

Hydrogels for dental pulp repair present a promising strategy to enhance physicochemical and regenerative potentials. This study focuses on a hydrogel matrix fabricated by combining alginate and gelatin, incorporating varying concentrations of calcium phosphate (CaP) at 0, 2, 4, and 6 wt% to evaluate their effects on the mechanical properties of hydrogels for dental pulp regeneration (DPR). Scanning electron microscopy (SEM) was employed to assess the morphological characteristics of the hydrogels. Additionally, finite element analysis (FEA) was introduced to model the conical nerve root, and an artificial neural network (ANN) model was developed to predict the relationships between composition and mechanical and biological properties. Results demonstrated that increasing CaP content enhanced tensile strength, reduced porosity, and improved pH stability, with optimal performance observed at 4 wt%. The ANN effectively explored the relationships among parameters influencing tensile strength and porosity, accurately predicting damage percentage, weight gain, and strut diameter. Linear regression analysis validated the ANN's predictions, indicating acceptable error margins relative to experimental data. Incorporation of 4 wt% CaP into the alginate-gelatin hydrogel significantly enhanced its mechanical properties, bioactivity, and stability, highlighting the potential of this novel bio-nanocomposite porous scaffold for DPR applications.

Keywords: *Dental pulp regeneration, Tissue engineering, Scaffolds, Hydrogels, Calcium phosphates, 3D bioprinting*

How to cite this article

Khademi A, Khandan A, Iranmanesh P. Hydrogels for dental pulp repair: enhancing physicochemical and regenerative potential with CaP-loaded alginate-gelatin hydrogel scaffolds: a FEM and ANN modeling. Nanomed J. 2026; 13(1): 183-195. DOI: 10.22038/NMJ.2025.84229.2115

INTRODUCTION

The quest for effective strategies in dental pulp regeneration (DPR) has garnered significant attention in regenerative medicine [1–2]. Dental pulp, a vital tissue at the tooth's center, is crucial in maintaining tooth vitality and overall oral health [2–3]. Damage to this tissue, caused by caries, trauma, or other pathological conditions, can lead to severe complications, including tooth loss [3–4]. Traditional treatment modalities often involve endodontic therapy, which may not fully restore the natural structure or function of the tooth. Therefore, innovative approaches promoting DPR are paramount [4–5]. One promising method involves using hydrogels, which have emerged as versatile biomaterials capable of supporting tissue engineering applications. Hydrogels are three-dimensional, hydrophilic polymer networks that retain large amounts of water while maintaining structural integrity [5–7].

This unique property enables hydrogels to mimic the natural extracellular matrix (ECM), providing a conducive environment for cell attachment, proliferation, and differentiation. The biocompatibility of hydrogels is a critical factor in their application for DPR. They must support cellular activities and interact favorably with the surrounding tissues to promote healing. Alginate, a naturally occurring polysaccharide derived from brown seaweed, is frequently used in hydrogel formulations due to its excellent biocompatibility, non-toxicity, and ability to form hydrogels via ionic cross-linking [8–11]. Alginate-based hydrogels can encapsulate various bioactive agents and cells, rendering them suitable for regenerative applications. Incorporating calcium phosphate (CaP) into alginate hydrogels has attracted considerable interest owing to the mineral's relevance in dental tissue regeneration [12–14]. Calcium phosphate compounds, including

* *Corresponding author:* Abbasali Khademi, Professor, Department of Endodontics, Dental Research Center, Dental Research Institute, School of Dentistry, Isfahan University of Medical Sciences, Isfahan, Iran. E-Mail address: *a_khademi@dnt.mui.ac.ir.*

Note. This manuscript was submitted on May 15, 2024; approved on August 14, 2024.

hydroxyapatite, are key constituents of natural bone and dentin, providing essential structural and functional properties for tissue regeneration. Incorporating CaP into alginate hydrogels can enhance their mechanical properties, bioactivity, and stability, thereby increasing their effectiveness for DPR. The interaction between alginate and CaP improves the hydrogel's physical characteristics and promotes mineralization and cellular activity, which are critical for successful pulp tissue regeneration [15–17]. Mechanical properties are a crucial consideration in the design of hydrogels for DPR. The hydrogel must possess sufficient strength and stability to withstand masticatory forces while maintaining flexibility to support natural tooth function. The mechanical behavior of alginate-CaP hydrogels is influenced by CaP concentration, alginate cross-linking density, and overall hydrogel architecture. Understanding the effects of these factors on mechanical properties is vital for optimizing hydrogel formulations for dental pulp applications [18–21]. In addition to mechanical properties, the biocompatibility of hydrogels is a fundamental factor determining their suitability for clinical applications. For DPR, hydrogels must facilitate cellular adhesion, proliferation, and differentiation while minimizing inflammatory responses. The inherent biocompatibility of alginate, combined with the bioactive properties of calcium phosphate, creates a favorable environment for DPR. Studies have demonstrated that incorporating bioactive additives, such as growth factors (GFs) and nanoparticles, into alginate-CaP hydrogels can further enhance their regenerative potential. These modifications promote cell signaling pathways that facilitate tissue repair and regeneration, thereby improving the overall efficacy of hydrogels as scaffolds for DPR. Hydrogels, particularly alginate-based formulations with calcium phosphate additives, represent a promising strategy for DPR. Their unique properties—including the ability to mimic the extracellular matrix (ECM), support cellular functions, and provide mechanical stability—make them ideal candidates for this application. Understanding the interplay between mechanical properties and biocompatibility is crucial for optimizing hydrogel formulations that effectively promote dental pulp tissue regeneration, with tools such as Artificial Neural Networks (ANNs) and Finite Element Analysis (FEA). As research in this field advances, the potential for hydrogels to revolutionize dental treatments becomes increasingly apparent, paving the way for more effective and regenerative solutions for dental pulp repair and oral health. A feedforward ANN with one hidden layer was employed to investigate and predict key parameters, including damage percentage (%), weight gain (%), and strut diameter (μm), based on a broad range of tensile strength (MPa) and porosity (%) as input variables. Additionally, linear regression was utilized to evaluate the error of the neural network. The ANN's predictions were analyzed, and the trends and accuracy of the estimates were thoroughly assessed.

MATERIALS AND METHODS

Preparation of CaP-Loaded Alginate-Gelatin hydrogels

Porous hydrogel scaffolds were fabricated using freeze-drying and 3D bioprinting techniques. High-G alginate (Mw 50–200 kDa, G/M ratio ≥ 0.6) and gelatin were obtained from Sigma-Aldrich, USA. Calcium chloride ($CaCl_2$), sodium phosphate dibasic (Na_2HPO_4), and sodium phosphate monobasic (NaH_2PO_4) were also purchased from Sigma-Aldrich. Alginate and gelatin were dissolved in deionized water at concentrations of 3% and 5% (w/v), respectively, and the solutions were mixed in a 1:1 ratio. A 3D scaffold design was created using SolidWorks software and fabricated via photopolymer light curing followed by freeze-drying. The prepared scaffolds were coated with 2, 4, or 6 wt% CaP-alginate layers. The 3D bioprinter used in this study was the Bio-Fab series model BioFabX2 (Omidafarinan, Iran). Varying concentrations of CaP (0, 2, 4, and 6 wt%) were added to the alginate-gelatin solution and homogenized to ensure uniform distribution. The CaP-loaded alginate-gelatin bioink was extruded through a 150–200 μm nozzle onto sterile petri dishes. The extruded hydrogel strands were crosslinked by immersion in a 100 mM $CaCl_2$ solution for 15–17 minutes. Finally, the 3D bioprinted hydrogel scaffolds were washed with phosphate-buffered saline (PBS) and stored in DMEM at 4°C until further use.

Physicochemical Characterization

The physicochemical properties of the CaP-loaded alginate-gelatin hydrogel scaffolds were evaluated using various techniques. Tensile mechanical properties were assessed using a dynamic mechanical analyzer at a 1 mm/min compression rate. The microstructure and pore size distribution of the CaP-loaded alginate-gelatin hydrogel scaffolds were analyzed by scanning electron microscopy (SEM; LEO, Netherlands).

Porosity Measurement

The porosity percentage of the CaP-loaded alginate-gelatin hydrogel scaffolds was determined using the Archimedes method. The scaffolds were immersed in deionized water for 5 hours at 37 ± 1°C, and porosity was calculated according to Equation 1:

$$P = (W-D)/(W-S) \times 100 \quad \text{(Equation 1)}$$

Where W is the wet weight of the scaffold after 24 hours of immersion in deionized water, D is the dry weight of the scaffold, and S is the weight of the scaffold while immersed in water.

Computational Modeling

In this study, multiple linear regression and artificial neural networks (ANNs) were utilized to develop predictive models for determining the optimal calcium phosphate (CaP) content in hydrogel scaffolds tailored for DPR. The analysis focused on various physicochemical and biological performance metrics, including pH change, degradation percentage, weight gain percentage, and strut diameter. Data distribution was visualized using histograms, facilitating a clearer understanding of relationships between variables. The performance of the ANN models was evaluated by comparing regression plots against the ideal y=x line, serving as a benchmark for predictive accuracy. The network error, derived from the linear regression analysis, was used as a metric to assess the predictive capability of the ANN models. To further explore the interrelationships among parameters, the ANN was employed to provide insights into how each variable influences the others. The network was trained to estimate degradation percentage, weight gain percentage, and strut diameter based on variations in tensile strength and porosity over a broader range than the experimental data. Predictions and analyses indicated that changes in tensile strength and porosity significantly impacted degradation, weight gain, and strut diameter outcomes. The error percentage in ANN predictions was assessed using linear regression, confirming that the model's error remained within acceptable limits compared to experimental results.

The study focused on predicting degradation, weight gain, and strut diameter across four experimental samples tested within compressive strength ranges of 0 to 1.75 MPa and porosity levels from 0% to 42%. A feedforward ANN was constructed with tensile strength and porosity as inputs, a single hidden layer comprising five neurons (following the guideline of twice the number of inputs plus one to enhance convergence), and outputs corresponding to degradation, weight gain, and strut diameter. The nonlinear sigmoid function was selected as the activation function due to its capability to model the nonlinear characteristics of the data, ensuring higher prediction accuracy and faster convergence. The error function was optimized using the gradient descent algorithm during training, and the input data were normalized before training to improve accuracy. After prediction, results were denormalized to validate their relevance within the expected range. To further evaluate the ANN's predictive performance, the fitted regression plot was compared against the ideal y=x line to assess accuracy. Network error was quantified through linear regression analysis, and predicted results were normalized to facilitate comparison. Finite Element Analysis (FEA) was also employed to investigate the mechanical behavior and stress distribution within calcium phosphate (CaP)-loaded alginate-gelatin hydrogel scaffolds. FEA is a powerful computational technique that enables the simulation and analysis of complex structures under various loading conditions. A three-dimensional conical nerve root structure model was developed using SolidWorks software, the basis for the FEA simulations. This model was subjected to a series of loading scenarios to evaluate scaffold performance under physiologically relevant conditions. The FEA assessed parameters such as strain, deformation, and stress within the hydrogel scaffolds, with both maximum and minimum values recorded and analyzed to comprehensively understand the material's mechanical response. This analysis was crucial for identifying the optimal CaP concentration that balances mechanical strength and flexibility, essential for effective DPR. The integration of FEA modeling and experimental data enabled the researchers to optimize the design and composition of CaP-loaded alginate-gelatin hydrogel scaffolds, ensuring their suitability for targeted DPR applications. Statistical analyses were performed using one-way analysis of variance (ANOVA), followed by Tukey's post-hoc test to assess the significance of the results. A p-value less than 0.05 was considered statistically significant. All experiments were conducted in triplicate, with results presented as mean ± standard deviation. Figure 1 illustrates a schematic of the alginate-gelatin-CaP hydrogel matrix designed for dental pulp repair and

regeneration, depicting the conceptual framework underlying the scaffold development approach.

Figure 1 illustrates the conceptual framework of the alginate-gelatin hydrogel matrix integrated with varying concentrations of calcium phosphate (CaP) for DPR. The schematic highlights the role of CaP concentration in enhancing the hydrogel's tensile strength, reducing porosity, and improving pH stability—key factors critical to successful DPR. Additionally, the diagram depicts the potential for cellular infiltration and nutrient exchange within the porous structure, which are essential for maintaining the vitality of regenerated dental pulp tissue.

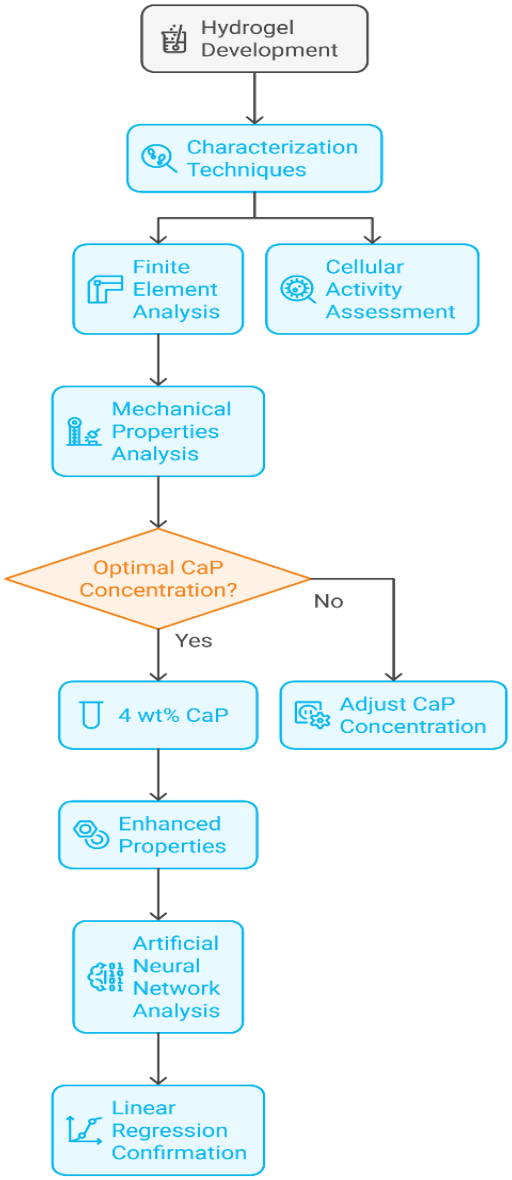

Fig. 1. Schematic representation of the alginate-gelatin-CaP hydrogel matrix for DPR

RESULTS AND DISCUSSION

Cells cultured in two-dimensional (2D) environments often exhibit random migration and misdirection, highlighting the necessity of three-dimensional (3D) culture for practical tissue engineering [11–14]. 3D culture better replicates the natural cellular microenvironment, facilitating improved colonization and extracellular matrix (ECM) formation. Tissue engineering scaffolds are designed to replace damaged cells while gradually degrading to support the regeneration of new tissue [15–16]. CaP-loaded alginate-gelatin hydrogel scaffolds must be biodegradable and non-toxic, with degradation rates synchronized to tissue regeneration to avoid the need for surgical removal [15–17]. Scaffold architecture is critical, requiring interconnected pores to permit cell infiltration and waste removal. Hydrogels, due to their high water absorption capacity, closely mimic living tissues and exhibit excellent biocompatibility. Recent advances in conductive polymers, such as polyaniline, have enhanced the mechanical properties of hydrogels and promoted tissue regeneration, making them promising candidates for applications including drug delivery and biosensing.

To predict changes in degradation (%), weight gain (%), and strut diameter (μm) with increasing compressive strength (MPa) and porosity (%), a FFANN was developed as described in Table 1. The model predicted and analyzed the degradation behavior, weight gain, and strut diameter across compressive strengths ranging from 0 to 1.72 MPa and porosity levels from 0 to 42%. Table 1 summarizes the mechanical properties—including weight fraction, tensile strength, porosity, pH changes, degradation, weight gain, and strut diameter—of four samples containing 0, 2, 4, and 6 wt% CaP.

The square-shaped structures printed using alginate-gelatin hydrogels may serve as scaffolds for various DPR applications, particularly in oral and dental therapies [10–12]. Integrating 3D bioprinting technology with alginate-based printed samples demonstrates the potential to fabricate personalized and complex tissue constructs for treating oral and dental diseases. The precise control over the geometry and composition of the printed structures enables the development of customized solutions tailored to individual patient needs [11–13]. The mechanical properties of the alginate-gelatin hydrogel scaffolds with varying CaP content are summarized in Table 1.

Table 1. Mechanical Properties of Alginate-Gelatin Hydrogels with Varying CaP Content

Samples	Weight fraction	Compressive Strength (MPa)	Porosity (%)	pH changes	Degradation (%)	Weight Gain (%)	Strut diameter (μm)
Sample 1	0 wt%	1.1	42	6.8	20	45	60
Sample 2	2 wt%	1.4	40	6.9	35	40	55
Sample 3	4 wt%	1.6	35	7.2	40	35	50
Sample 4	6 wt%	1.75	30	6.9	45	38	45

Table 1 demonstrates that as the CaP weight fraction increases from 0 wt% to 6 wt%, the tensile strength of the hydrogel samples rises from 1.1 MPa to 1.75 MPa, while porosity decreases from 42% to 30%. This trend suggests that incorporating CaP nanoparticles into the alginate-gelatin hydrogel matrix enhances the mechanical strength of the scaffolds, likely due to the reinforcement effect of the CaP particles. Figure 2 (a–d) presents SEM images illustrating the surface morphology of CaP-loaded alginate-gelatin hydrogel scaffolds with varying CaP weight percentages. In Figure 2(a), the scaffold exhibits a relatively smooth and uniform surface, corresponding to a low CaP concentration and limited porosity, which may hinder cellular infiltration and nutrient exchange. With increasing CaP content, significant changes in surface morphology are observed. Figure 2(b) shows a more porous and rougher texture, reflecting improved porosity that could facilitate enhanced cell adhesion and proliferation. Figure 2(c) reveals a distinctly porous and interconnected network, promoting cellular infiltration and nutrient diffusion, both essential for maintaining cell viability. Figure 2(d) illustrates a highly porous, sponge-like surface structure, indicating a substantial increase in CaP content within the alginate-gelatin hydrogel scaffolds. This enhanced porosity increases the surface area, facilitating greater interaction with cells and bioactive molecules. Furthermore, the observed reduction in porosity across the SEM images correlates with the data presented in Table 1, highlighting the relationship between CaP concentration and scaffold morphology. These results show the importance of scaffold characteristics in optimizing functionality for DPR. The progressive surface texture and porosity changes provide compelling evidence of how varying CaP concentrations influence scaffold design and performance.

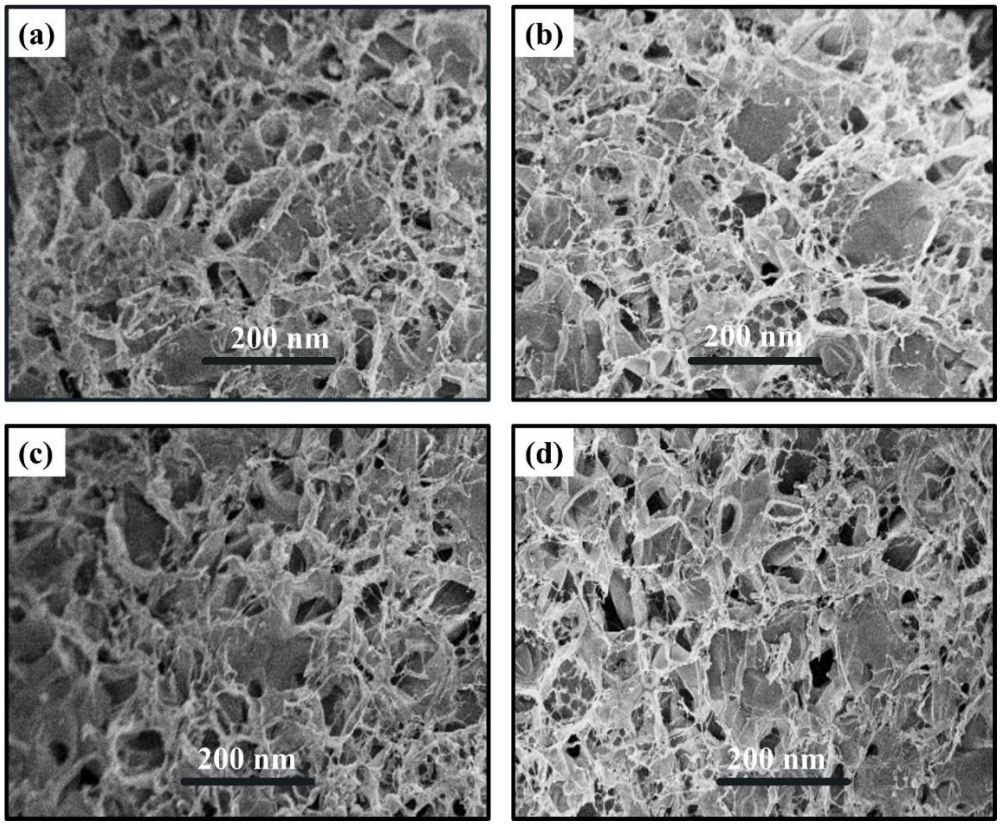

Fig. 2. SEM image of alginate-gelatin scaffold surface containing a) 0 wt%, b) 2 wt%, c) 4 wt%, and d) 6 wt% CaP

SEM analysis of freeze-dried scaffolds reveals a regular morphology with pore sizes ranging from approximately 50 to 70 nm, which is essential for tissue engineering because it enhances nutrient exchange and maintains structural integrity. The freeze-drying process allows precise control over pore size, effectively mimicking the natural extracellular matrix (ECM). Additionally, Finite Element Analysis (FEA) and Artificial Neural Network (ANN) modeling demonstrate appropriate mechanical behavior and favorable biological responses, optimizing the performance of CaP-loaded alginate-gelatin hydrogel scaffolds for DPR. SEM images of the scaffold surface morphology show an amorphous and porous structure with approximately 7 and 10 micrometers of pore sizes. The surface architecture indicates covalent bonding among the scaffold components, resulting in a complex, interconnected microstructure. Distinct boundaries between individual particles or building blocks are visible, suggesting a well-defined and cohesive structure. The surface topography also reveals open pores with diameters ranging from 10 to 15 microns. This porous network will likely facilitate cell infiltration, nutrient transport, and waste removal—critical factors for successful DPR applications [20–24]. The design and properties of CaP-loaded alginate-gelatin hydrogel scaffolds are essential for the successful integration and functional recovery of target tissues [25–27]. The researchers showed ANN techniques to model the relationships between CaP content and the scaffold's mechanical properties. This approach enabled the prediction of optimal CaP loading to achieve desired mechanical characteristics, demonstrating the effectiveness of integrating advanced computational modeling with experimental data [28–32]. Furthermore, the ANN models were utilized to estimate other key parameters such as pH change, degradation, weight gain, and initial strut diameter, based on weight fraction, tensile strength, and porosity. The accuracy of these predictions was validated through linear regression analysis, confirming the reliability of the ANN-based methodology.

The results demonstrated that increasing the CaP content in the alginate-gelatin hydrogel scaffold improved tensile strength, reduced porosity, and enhanced pH stability, while promoting degradation and weight gain. The optimal CaP loading was identified as 4 wt%, as this formulation exhibited superior mechanical properties, bioactivity, and stability compared to other compositions. Incorporation of 4 wt% CaP into the alginate-gelatin hydrogel matrix underscores the potential of this nanocomposite scaffold for DPR applications. Moreover, 3D bioprinting enables precise spatial placement of living cells, biological materials, and growth factors, effectively mimicking native tissue architecture. This technique overcomes limitations of traditional scaffold fabrication methods, such as insufficient mechanical strength and rapid dissolution rates [33–35]. Additionally, incorporation of nanomaterials like graphene oxide has been shown to enhance cell adhesion, proliferation, and osteogenic differentiation within 3D-printed scaffolds [36–40]. In this study, we developed an ANN model to predict changes in pH, degradation (%), weight gain (%), and diameter (µm) based on increasing weight fraction, tensile strength (MPa), and porosity (%) using data presented in Table 1. The behavior of these parameters was investigated within specified ranges of weight fraction (0–6%), compressive strength (0–1.75 MPa), and porosity (0–42%). Figure 3 illustrates the ANN architecture, comprising a hidden layer with five neurons and two inputs—tensile strength (MPa) and porosity (%)—across four samples, designed to predict degradation (%), weight gain (%), and strut diameter (µm).

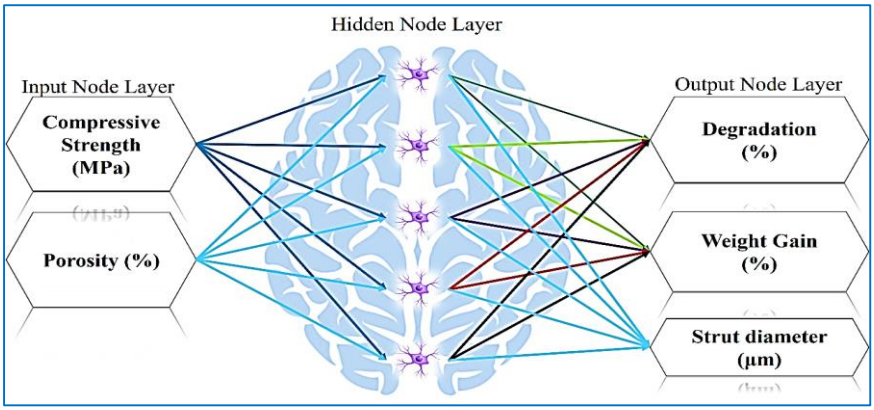

Fig. 3. Schematic of an ANN with a hidden layer, a study on alginate-gelatin hydrogels with calcium phosphate additives and optimization of ANN modeling for DPRs

Figures 4(a–b) present the degradation change predictions made by the ANN. The results indicate that increasing porosity percentage leads to a decrease in degradation. Conversely, increasing tensile strength is associated with a positive and increasing trend in degradation.

Figures 5(a–b) depict the ANN-predicted changes in weight gain. The analysis suggests that higher porosity percentages contribute to increased weight gain.

Additionally, weight gain remains constant with changes in tensile strength from 0 to 1 MPa, after which it exhibits a positive and increasing trend. Figures 6(a–b) present the ANN-predicted changes in strut diameter. The results suggest that increasing porosity leads to a generally stable and slightly positive trend in strut diameter.

An increase in tensile strength causes a decrease in strut diameter. The results of the linear regression analysis relating inputs to outputs are shown in Figure 7(a–c). The ANN was able to predict degradation (%), weight gain (%), and strut diameter (µm) with very high accuracy, achieving an error of less than 1% compared to the target values presented in Table 1.

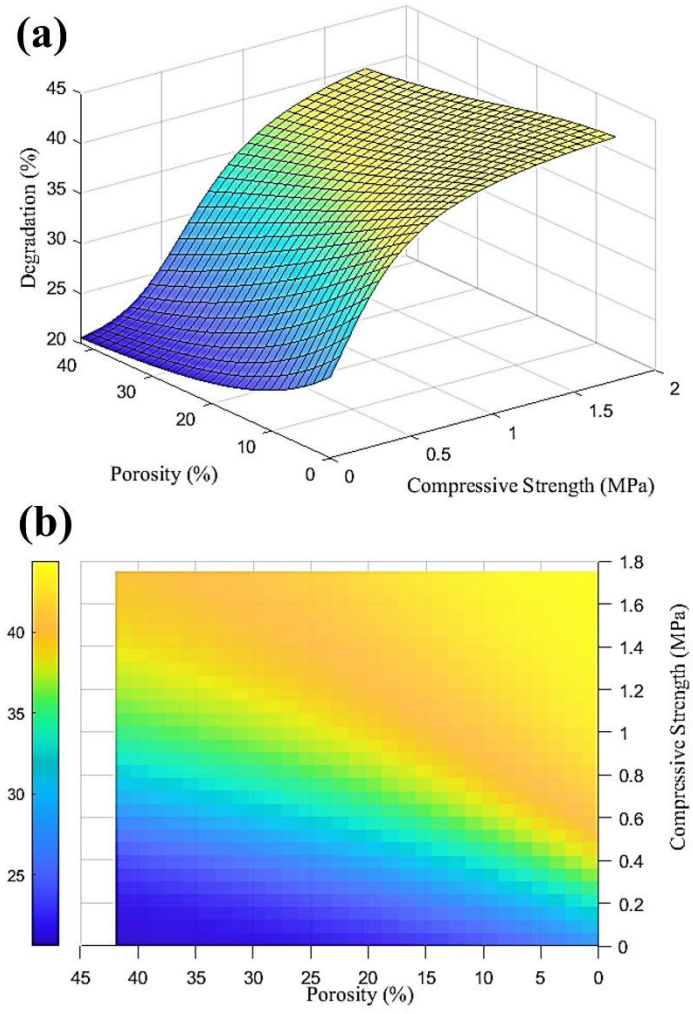

Fig. 4. Prediction made by the ANN to predict the degradation of the test item a) front view and b) side view

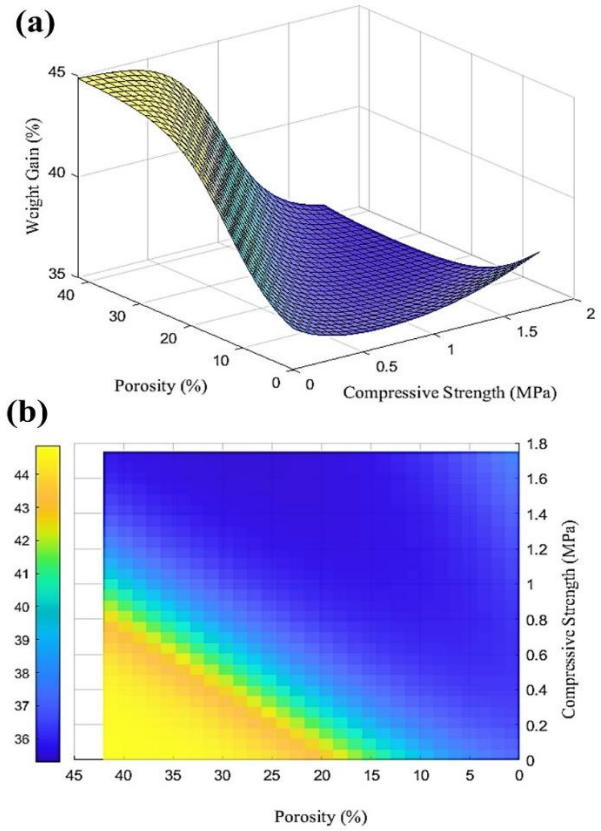

Fig. 5. Prediction made by the ANN to predict the weight gain of the test item a) front view and b) side view

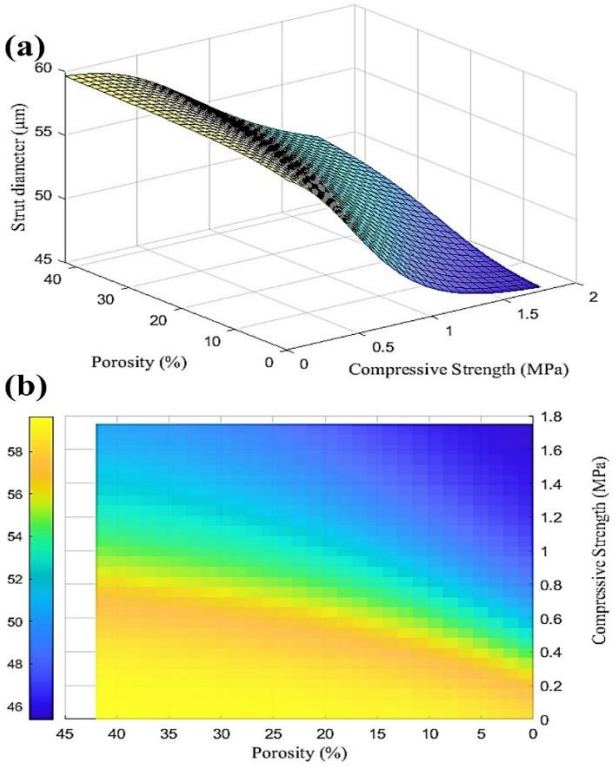

Fig. 6. Prediction made by the ANN to predict the diameter of the test item a) front view and b) side view

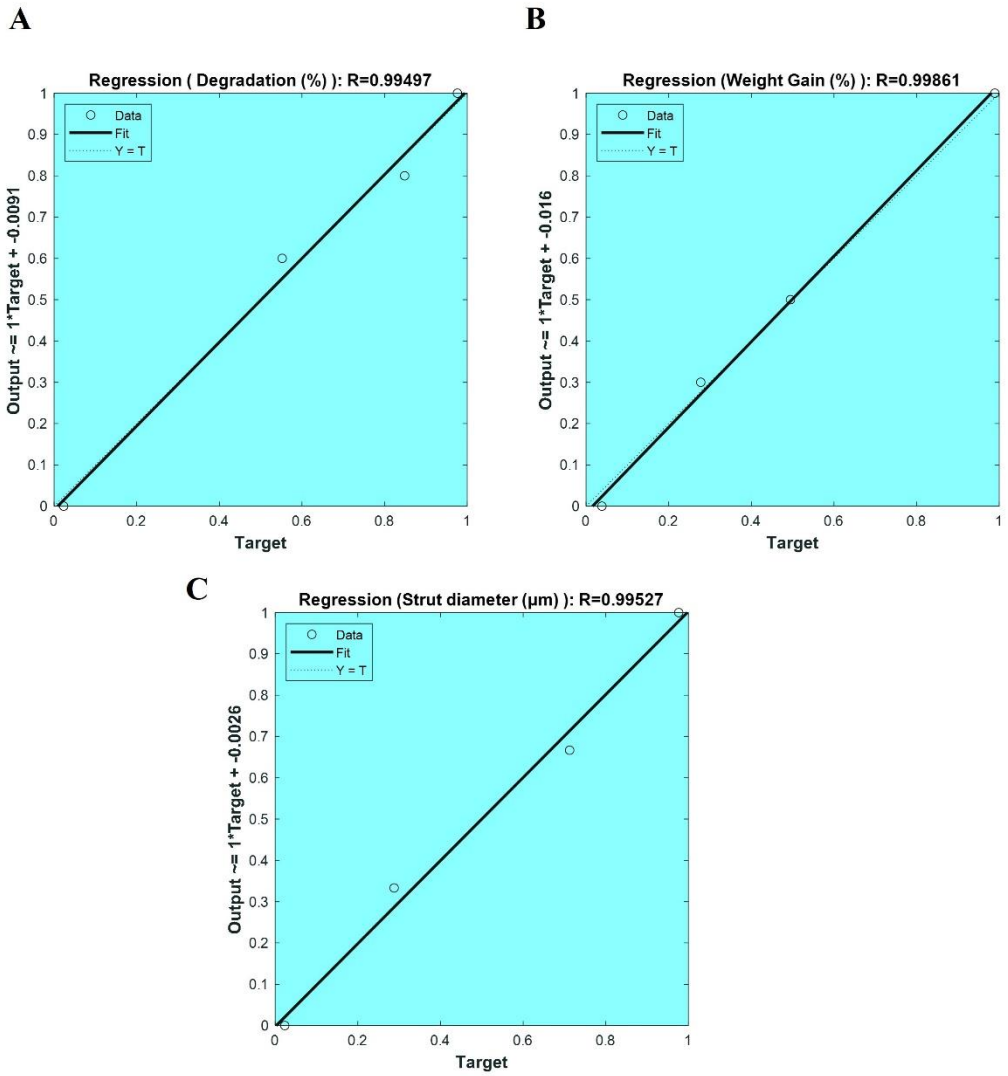

Fig. 7. Linear regression plots to examine the error of the ANN formed for a) degradation (%), b) weight gain (%) and c) diameter of the test item (µm)

Figure 8 presents the strain values observed under maximum and minimum loading conditions. The maximum strain recorded is 166.54 Pa, indicating a significant level of deformation experienced by the material under load. The minimum strain is 0.0014 Pa, suggesting that some material areas undergo negligible deformation. This wide range of strain values reflects the material's heterogeneous response to applied forces, which can be attributed to material composition, structural design, and external loading conditions. The ability to withstand varying strain levels is crucial for materials used in load-bearing applications because it directly impacts their reliability and longevity.

Figure 9 shows deformation values in meters to quantitatively assess how much the material is displaced under stress. The maximum deformation is noted at 0.059 m, while the minimum deformation is recorded at 0 m. These data determine how much the material can deform before reaching its elastic limit or yielding point. The maximum deformation value shows that the material can accommodate significant displacement, which may be advantageous in applications requiring flexibility and adaptability. The minimum deformation indicates that certain conditions or areas within the material remain stable, contributing to structural integrity. Understanding deformation behavior is essential for predicting material performance under real-world, dynamic conditions where forces fluctuate.

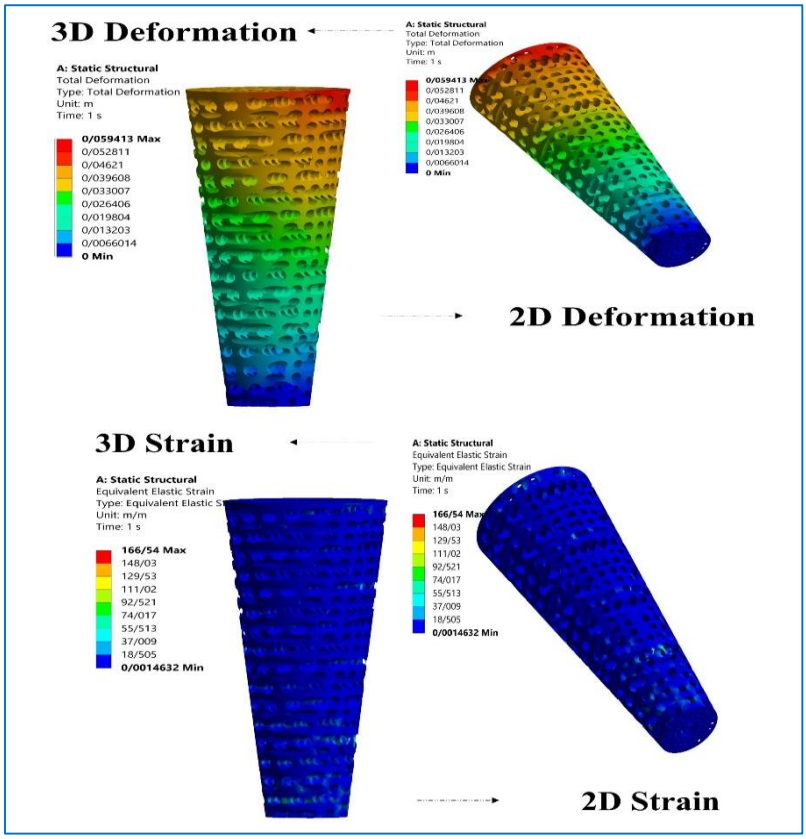

Fig. 8. Analysis of strain values under maximum and minimum states, measured in Pascals. The maximum strain recorded is 166/54 Pa, while the minimum strain is 0.0014 Pa

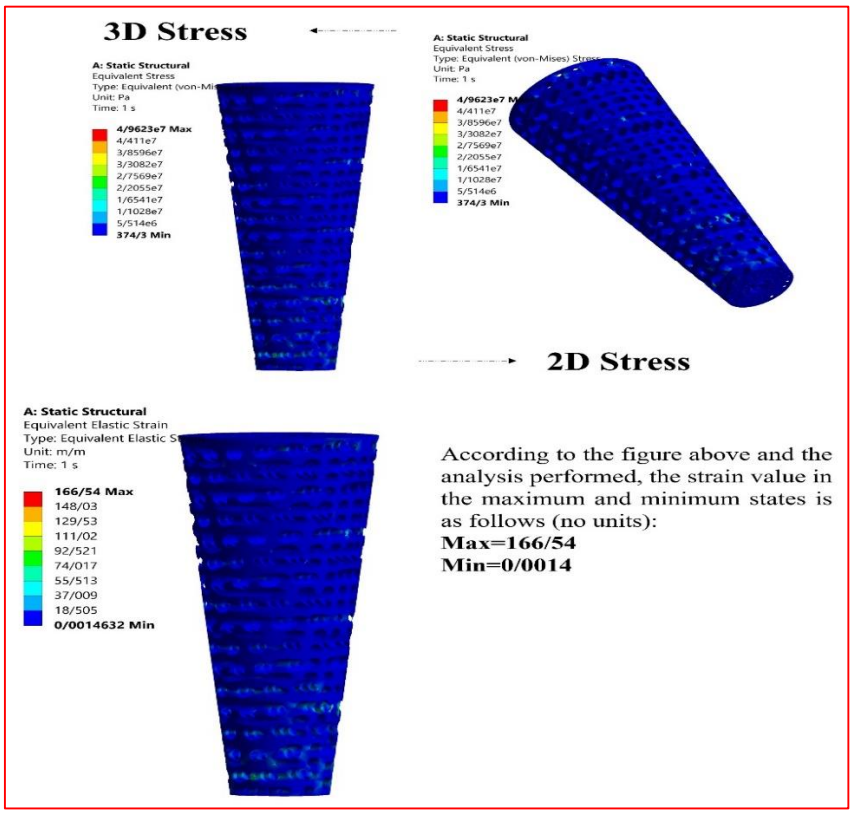

Fig. 9. Deformation values observed in the system during analysis, measured in meters. The maximum deformation is noted at 0.059 m

Figure 10 illustrates the stress values analyzed under maximum and minimum states. The maximum stress was 4.9623e7 Pa, while the minimum was 374.3 Pa. These values are instrumental in assessing the material's strength and capacity to withstand external loads without experiencing failure. The high maximum stress value indicates that the material can withstand significant forces, reflecting robust mechanical properties suitable for demanding applications. In contrast, the minimum stress value represents regions experiencing low external loading, an essential consideration in material design and safety. Understanding the relationships between strain, deformation, and stress is fundamental to characterizing material behavior. Strain provides insight into the extent of material deformation under stress, while stress quantifies the internal forces generated within the material in response to external loads.

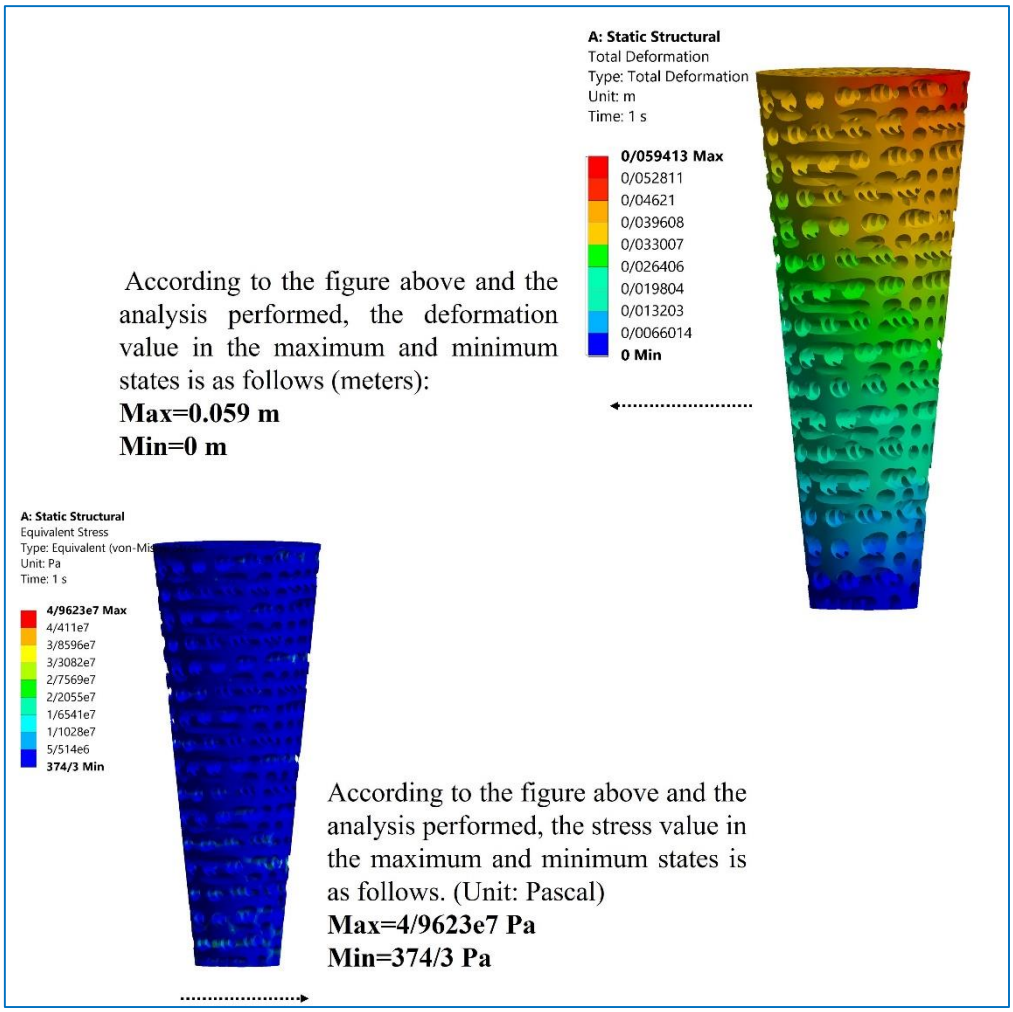

Fig. 10. Stress values analyzed under maximum and minimum states, expressed in Pascals. The maximum stress is measured at 4.9623e7 Pa, while the minimum stress is 374.3 Pa

CONCLUSION

This study developed a porous, bio-printed alginate-gelatin hydrogel scaffold loaded with varying calcium phosphate (CaP) concentrations for dental pulp tissue engineering. Incorporation of CaP significantly enhanced the scaffold's physicochemical and mechanical properties, with tensile strength increasing from 1.1 MPa to 1.75 MPa and porosity decreasing from 42% to 30% as CaP content rose from 0 wt% to 6 wt%. SEM analysis revealed that higher CaP concentrations produced more porous and interconnected surface morphologies, promoting cell infiltration, nutrient transport, and waste removal—key factors for effective tissue regeneration. The optimal CaP concentration was identified as 4 wt%, which provided the best balance of mechanical strength, bioactivity, and stability. Computational modeling techniques, including ANNs, were employed to predict the ideal CaP loading for desired mechanical characteristics and parameters such as pH, degradation, weight gain, and strut diameter. The

reliability of these predictions was confirmed through linear regression analysis, highlighting the value of integrating computational methods with experimental research. The scaffold developed with 4 wt% CaP shows great promise for DPR, with enhanced mechanical and biological properties expected to improve dental pulp restoration and repair.

AVAILABILITY OF DATA AND MATERIALS

The datasets supporting the conclusions are included within the article.

COFLICTS OF INTEREST

The authors have declared no competing interests.

ACKNOWLEDGEMENT

This research project was supported by a grant from the Dental Research Center, Dental Research Institute, School of Dentistry, Isfahan University of Medical Sciences, Isfahan, Iran (Grant No. IR.MUI.RESEARCH.REC.1401.203 and Scientific Research Proposal of 240169). Also, it should be mentioned that A. Khandan and A. Khademi contributed equally to this work.

REFERENCES

1. Eramo S, Natali A, Pinna R, Milia E. Dental pulp regeneration via cell homing. Int End J. 2018;51(4):405-419.
2. Khademi A, Khandan A, Iranmanesh P, Heydari M. Development of a 3D Bioprinted Alginate-Gelatin Hydrogel Scaffold Loaded with Calcium Phosphates for Dental Pulp Tissue Regeneration. IJCCE. 2024.
3. Xie Z, Shen Z, Zhan P, Yang J, Huang Q, Huang S, Chen L, Lin Z. Functional dental pulp regeneration: basic research and clinical translation. Int J Mol Sci. 2021;22(16):8991.
4. Khandan A, Khosravi M, Roustazadeh D, Aghadavoudi F. Impact of alumina and carbon nanotubes on mechanical properties of a composite: molecular dynamic (MD) simulation. IJCCE, (Articles in Press). 2024.
5. Itoh Y, Sasaki JI, Hashimoto M, Katata C, Hayashi M, Imazato S. Pulp regeneration by 3-dimensional dental pulp stem cell constructs. J Dent Res. 2018;97(10):1137-1143.
6. An J, Chua CK, Mironov V. Application of machine learning in 3D bioprinting: focus on development of big data and digital twin. Int J Bioprint. 2021;7(1).
7. Ng WL, Yeong WY, Naing MW. Polyelectrolyte gelatin-chitosan hydrogel optimized for 3D bioprinting in skin tissue engineering. Int J Bioprint. 2016;2(1):53-62.
8. Zhang R, Xie L, Wu H, Yang T, Zhang Q, Tian Y, Liu Y, Han X, Guo W, He M, Liu S. Alginate/laponite hydrogel microspheres co-encapsulating dental pulp stem cells and VEGF for endodontic regeneration. Acta Biomater. 2020;113:305-316.
9. Yu H, Zhang X, Song W, Pan T, Wang H, Ning T, Wei Q, Xu HH, Wu B, Ma D. Effects of 3-dimensional bioprinting alginate/gelatin hydrogel scaffold extract on proliferation and differentiation of human dental pulp stem cells. J Endod. 2019;45(6):706-715.
10. Bhoj M, Zhang C, Green DW. A first step in de novo synthesis of a living pulp tissue replacement using dental pulp MSCs and tissue growth factors, encapsulated within a bioinspired alginate hydrogel. J Endod. 2015;41(7):1100-1107.
11. Bendtsen ST, Quinnell SP, Wei M. Development of a novel alginate-polyvinyl alcohol-hydroxyapatite hydrogel for 3D bioprinting bone tissue engineered scaffolds. J Biomed Mater Res Part A. 2017;105(5):1457-1468.
12. Rad MM, Saber-Samandari S, Sadighi M, Tayebi L, Aghdam MM, Khandan A. Macro-and micromechanical modelling of HA-Elastin scaffold fabricated using freeze drying technique. J Nanoanal. 2021.
13. Al-Sanabani JS, Madfa AA, Al-Sanabani FA. Application of calcium phosphate materials in dentistry. Int J Biomater. 2013;2013(1):876132.
14. Dorozhkin SV, Epple M. Biological and medical significance of calcium phosphates. Angew Chem Int Ed. 2002;41(17):3130-3146.
15. Ching SH, Bansal N, Bhandari B. Alginate gel particles–A review of production techniques and physical properties. Crit Rev Food Sci Nutr. 2017;57(6):1133-1152.
16. Potiwiput S, Tan H, Yuan G, Li S, Zhou T, Li J, Jia Y, Xiong D, Hu X, Ling Z, Chen Y. Dual-crosslinked alginate/carboxymethyl chitosan hydrogel containing in situ synthesized calcium phosphate particles for drug delivery application. Mater Chem Phys. 2020;241:122354.
17. Kengla C, Kidiyoor A, Murphy SV. Bioprinting complex 3D tissue and organs. In Kidney Transplantation, Bioengineering and Regeneration. Academic Press. 2017; 957-971.
18. Ananth KP, Jayram ND. A comprehensive review of 3D printing techniques for biomaterial-based scaffold fabrication in bone tissue engineering. Ann 3D Printed Med. 2024;13:100141.
19. Zhao X, Li N, Zhang Z, Hong J, Zhang X, Hao Y, Wang J, Xie Q, Zhang Y, Li H, Liu M. Beyond hype: unveiling the Real challenges in clinical translation of 3D printed bone scaffolds and the fresh prospects of bioprinted organoids. J Nanobiotechnol. 2024;22(1):500.
20. Golzar H, Mohammadrezaei D, Yadegari A, Rasoulianboroujeni M, Hashemi M, Omidi M, Yazdian F, Shalbaf M, Tayebi L. Incorporation of functionalized reduced graphene oxide/magnesium nanohybrid to enhance the osteoinductivity capability of 3D printed calcium phosphate-based scaffolds. Compos Part B Eng. 2020;185:107749.
21. Unagolla JM, Jayasuriya AC. Enhanced cell functions on graphene oxide incorporated 3D printed polycaprolactone scaffolds. Mater Sci Eng C. 2019;102:1-1.
22. Sharma A, Gupta S, Sampathkumar TS, Verma RS. Modified graphene oxide nanoplates reinforced 3D

printed multifunctional scaffold for bone tissue engineering. Biomat Adv. 2022;134:112587.
23. Iranmanesh P, Torabinejad M, Saatchi M, Toghraie D, Razavi SM, Khademi A. Effect of duration of root canal infection on the ability of dentin-pulp complex regeneration of immature permanent teeth: an animal study. J Endod. 2022;48(10):1301-1307.
24. Iranmanesh P, Gowdini M, Khademi A, Dehghani M, Latifi M, Alsaadi N, Hemati M, Mohammadi R, Saber-Samandari S, Toghraie D, Khan A. Bioprinting of three-dimensional scaffold based on alginate-gelatin as soft and hard tissue regeneration. J Mater Res Technol. 2021;14:2853-2864.
25. Iranmanesh P, Ehsani A, Khademi A, Asefnejad A, Shahriari S, Soleimani M, Ghadiri Nejad M, Saber-Samandari S, Khandan A. Application of 3D bioprinters for dental pulp regeneration and tissue engineering (porous architecture). Transp Porous Med. 2022;142(1):265-293.
26. Fatalla AA, Arzani S, Veseli E, Khademi A, Khandan A, Fahmy MD, Mirmohammadi H, Hasselgren G, Bang H, Kolahi J, Kelishadi R. Revolutionizing systematic reviews and meta-analyses: the role of artificial intelligence in evidence synthesis. Dent Hypotheses. 2023;14(4):93-94.
27. Khandan A, Jazayeri H, Fahmy MD, Razavi M. Hydrogels: Types, structure, properties, and applications. Biomed Tissue Eng. 2017;4(27):143-169.
28. Mashhadi Keshtiban M, Taghvaei H, Noroozi R, Eskandari V, Arif ZU, Bodaghi M, Bardania H, Hadi A. Biological and Mechanical Response of Graphene Oxide Surface-Treated Polylactic Acid 3D-Printed Bone Scaffolds: Experimental and Numerical Approaches. Adv Eng Mater. 2024;26(3):2301260.
29. Wei Y, Pan H, Yang J, Zeng C, Wan W, Chen S. Aligned cryogel fibers incorporated 3D printed scaffold effectively facilitates bone regeneration by enhancing cell recruitment and function. Sci Adv. 2024;10(6):eadk6722.
30. Geng Y, Liu T, Zhao M, Wei H, Yao X, Zhang Y. Silk fibroin/polyacrylamide-based tough 3D printing scaffold with strain sensing ability and chondrogenic activity. Compos Part B Eng. 2024;271:111173.
31. Rodriguez G, Dias J, d'Ávila MA, Bártolo P. Influence of hydroxyapatite on extruded 3D scaffolds. Proc Eng. 2013;59:263-269.
32. Lau D, Jian W, Yu Z, Hui D. Nano-engineering of construction materials using molecular dynamics simulations: Prospects and challenges. Compos Part B Eng. 2018;143:282-291.
33. Attaeyan A, Shahgholi M, Khandan A. Fabrication and characterization of novel 3D porous Titanium-6Al-4V scaffold for orthopedic application using selective laser melting technique. IJCCE. 2023;21-37.
34. Nouri A, Rabbath J, Khademi A, Khandan A, Iranmanesh P, Fahmy M. Reconstruction of Pathology Induced Anterior Maxillary Defect: A Case Report. Sci Hypotheses. 2024;1:72-78.
35. Maghsoudlou MA, Nassireslami E, Saber-Samandari S, Khandan A. Bone regeneration using bio-nanocomposite tissue reinforced with bioactive nanoparticles for femoral defect applications in medicine. Avicenna J Med Biotechnol. 2020;12(2):68.
36. Jasemi A, Moghadas BK, Khandan A, Saber-Samandari S. A porous calcium-zirconia scaffolds composed of magnetic nanoparticles for bone cancer treatment: Fabrication, characterization and FEM analysis. Ceram Int. 2022;48(1):1314-25.
37. Gašparovič M, Jungová P, Tomášik J, Mriňáková B, Hirjak D, Timková S, Danišovič Ľ, Janek M, Bača Ľ, Peciar P, Thurzo A. Evolving Strategies and Materials for Scaffold Development in Regenerative Dentistry. Appl Sci. 2024;14(6):2270.
38. Khademi A, Khandan A, Iranmanesh P, Heydari M. Development of a 3D Bioprinted Alginate-Gelatin Hydrogel Scaffold Loaded with Calcium Phosphates for Dental Pulp Tissue Regeneration. IJCCE. 2024.
39. Anaya-Sampayo LM, García-Robayo DA, Roa NS, Rodriguez-Lorenzo LM, Martínez-Cardozo C. Platelet-rich fibrin (PRF) modified nano-hydroxyapatite/chitosan/gelatin/alginate scaffolds increase adhesion and viability of human dental pulp stem cells (DPSC) and osteoblasts derived from DPSC. Int J Biol Macromol. 2024;133064.
40. Amiryaghoubi N, Fathi M, Safary A, Javadzadeh Y, Omidi Y. In situ forming alginate/gelatin hydrogel scaffold through Schiff base reaction embedded with curcumin-loaded chitosan microspheres for bone tissue regeneration. Int J Biol Macromol. 2024;256:128335.